

A 2.8 Å Fe–Fe Separation in the Fe₂^{III/IV} Intermediate, X, from *Escherichia coli* Ribonucleotide Reductase

Laura M. K. Dassama,^{†,‡,§} Alexey Silakov,[†] Courtney M. Krest,^{†,#} Julio C. Calixto,[†] Carsten Krebs,^{*,†,‡} J. Martin Bollinger, Jr.,^{*,†,‡} and Michael T. Green^{*,†}

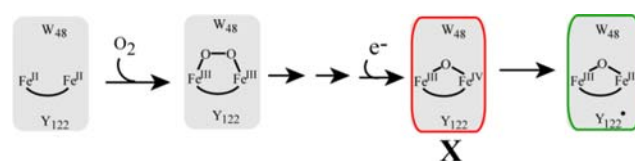
Departments of [†]Chemistry and [‡]Biochemistry and Molecular Biology, The Pennsylvania State University, University Park, Pennsylvania 16802, United States

S Supporting Information

ABSTRACT: A class Ia ribonucleotide reductase (RNR) employs a μ -oxo-Fe₂^{III/III}/tyrosyl radical cofactor in its β subunit to oxidize a cysteine residue ~ 35 Å away in its α subunit; the resultant cysteine radical initiates substrate reduction. During self-assembly of the *Escherichia coli* RNR- β cofactor, reaction of the protein's Fe₂^{II/II} complex with O₂ results in accumulation of an Fe₂^{III/IV} cluster, termed X, which oxidizes the adjacent tyrosine (Y₁₂₂) to the radical (Y₁₂₂[•]) as the cluster is converted to the μ -oxo-Fe₂^{III/III} product. As the first high-valent non-heme-iron enzyme complex to be identified and the key activating intermediate of class Ia RNRs, X has been the focus of intensive efforts to determine its structure. Initial characterization by extended X-ray absorption fine structure (EXAFS) spectroscopy yielded a Fe–Fe separation ($d_{\text{Fe–Fe}}$) of 2.5 Å, which was interpreted to imply the presence of three single-atom bridges (O²⁻, HO⁻, and/or μ -1,1-carboxylates). This short distance has been irreconcilable with computational and synthetic models, which all have $d_{\text{Fe–Fe}} \geq 2.7$ Å. To resolve this conundrum, we revisited the EXAFS characterization of X. Assuming that samples containing increased concentrations of the intermediate would yield EXAFS data of improved quality, we applied our recently developed method of generating O₂ *in situ* from chlorite using the enzyme chlorite dismutase to prepare X at ~ 2.0 mM, more than 2.5 times the concentration realized in the previous EXAFS study. The measured $d_{\text{Fe–Fe}} = 2.78$ Å is fully consistent with computational models containing a (μ -oxo)₂-Fe₂^{III/IV} core. Correction of the $d_{\text{Fe–Fe}}$ brings the experimental data and computational models into full conformity and informs analysis of the mechanism by which X generates Y₁₂₂[•].

Ribonucleotide reductases (RNRs) catalyze the conversion of ribonucleotides to deoxyribonucleotides, providing all organisms with precursors for the *de novo* synthesis and repair of DNA.¹ All RNRs identified to date utilize a free-radical mechanism. A transient cysteine thiyl radical (C[•]),² generated *in situ* in the first step of the reaction, abstracts a H atom from the 3'-position of the bound nucleotide. The mechanism by which the C[•] is generated in each turnover is the basis for the division of RNRs into classes I–III.¹

Scheme 1. Schematic Description of the Activation of *Ec* Class Ia RNR (X Is the Precursor to the Active Fe₂^{III/III}/Y[•] Cofactor)



A class Ia RNR, such as the prototypical orthologue from aerobically-growing *Escherichia coli* (*Ec*), functions as a 1:1 complex of homodimeric subunits, α_2 and β_2 . The α subunit binds substrates and allosteric effectors and contains the C residue (C₄₃₉ in *Ec* RNR) that is oxidized to the C[•], whereas the β subunit self-assembles a μ -oxo-Fe₂^{III/III}/tyrosyl radical cofactor that functions to generate the C[•] reversibly in each catalytic cycle.³ The functional cofactor is produced by reaction of the Fe₂^{II/II} complex of β with O₂ (Scheme 1).⁴ Addition of O₂ yields a μ -peroxo-Fe₂^{III/III} (P) complex⁵ that is reduced upon cleavage of the O–O bond of the peroxo moiety. In the *Ec* β reaction, the O–O cleavage step results in the one-electron oxidation of the solvent-accessible W₄₈ to a cation radical (W₄₈⁺)⁶ with concomitant formation of an Fe₂^{III/IV} form of the diiron cluster termed cluster X.⁷ The *Ec* W₄₈⁺ can be reduced *in vitro* by small-molecule reductants including ascorbate and thiols,⁶ but it is possible that an accessory protein serves as the reductant *in vivo*.⁸ The decay of the W₄₈⁺ leaves X to oxidize the nearby Y₁₂₂ residue to the stable Y₁₂₂[•]. In the process, X is reduced to the μ -oxo-Fe₂^{III/III} cluster of the active β subunit.^{4,7,9} The Y[•] is strictly conserved among all class Ia and Ib RNRs and is absolutely required for their activity.^{1a,3a,10}

The importance of X to the function of class Ia RNRs (which include the *Homo sapiens* orthologue) has made it a prime target for structural characterization. For *Ec* RNR, the rapid rate at which X decays (~ 1 s⁻¹ in the wild-type β ; 0.2 s⁻¹ in the Y₁₂₂F variant at 5 °C^{7,9}) has thus far prevented characterization by X-ray crystallography. Instead, the freeze-quench technique has been used to trap the intermediate, which has then been characterized by a variety of spectroscopic methods.^{9,11} Density functional theory (DFT) calculations have afforded models for its diiron core, and these models have been evaluated for consistency with the spectroscopic data.¹² This approach, now commonplace in investigations of reactive metalloenzyme

Received: July 19, 2013

Published: October 4, 2013

intermediates,¹³ has failed to forge a consensus regarding the structure of X, primarily because the short Fe–Fe separation ($d_{\text{Fe–Fe}} \approx 2.5 \text{ \AA}$)^{11e} of the intermediate determined by extended X-ray absorption fine structure (EXAFS) spectroscopy seemingly requires a structure with three single-atom bridges provided by some combination of the protein carboxylate ligands and O₂/solvent-derived hydr(oxo) ligands. Such a structure has been disfavored in computational studies on energetic grounds. Indeed, structures favored in these studies have had values of $d_{\text{Fe–Fe}} \geq 2.7 \text{ \AA}$ and no more than two single-atom O bridges.^{11b,12b–d} Furthermore, none of the available synthetic models for X has had such a short $d_{\text{Fe–Fe}}$.¹⁴ Additionally, structural metrics determined by EXAFS for a Mn^{IV}/Fe^{III} homologue of X in the RNR from *Chlamydia trachomatis* agree with those derived by DFT,¹⁵ indicating that current DFT methods are capable of accurately predicting the structures of such enzyme-bound dinuclear complexes.

We sought to resolve the conundrum concerning the structure of X by revisiting the irreconcilably short $d_{\text{Fe–Fe}}$ determined in the initial EXAFS study. The kinetics of the activation reaction preclude trapping of X in pure form, with a maximum fraction of ~ 0.7 having been achieved in published studies. The challenging kinetics had conspired with the poor solubility of O₂ in aqueous solutions ($< 2 \text{ mM}$ at 1 atm) to limit the concentration of X that could be trapped to $< 0.8 \text{ mM}$. Recent technological advancements now permit accumulation of O₂-derived intermediates at concentrations exceeding 2 mM,¹⁶ and we reasoned that the ability to trap X at elevated concentrations might yield samples of higher quality to permit the recharacterization of the intermediate by EXAFS spectroscopy.

Samples for this study were prepared by the method of generating O₂ *in situ* from chlorite (ClO₂[−]) with the enzyme chlorite dismutase (Cld).¹⁶ A reactant solution containing a high concentration of the preformed Fe₂^{II/II} complex of *Ec* RNR- β -Y₁₂₂F and a catalytic concentration (12.5 μM) of Cld was mixed with 0.25 equivalent volumes of a second reactant solution containing ClO₂[−], and the reaction was freeze-quenched after 0.3 s (at 5 °C). The 4.2-K/53-mT Mössbauer spectra of the freeze-quenched samples reveal the presence of $\sim 65\%$ X, comparable to the maximum fraction obtained in the previous EXAFS study, along with $\sim 18\%$ unreacted Fe^{II} species and $\sim 18\%$ of μ -oxo-Fe₂^{III/III} product cluster (Figures S1–S3, Supporting Information). This fraction of X corresponds to 2.0 mM, more than 2.5 times the maximum concentration attained in the previous EXAFS-spectroscopic study.

The X-ray absorption near-edge structure (XANES) spectra (Figure S4) show a higher K-edge absorption energy (the energy at which the 1s-core electron is ejected) for samples containing X than for the samples of the unreacted Fe₂^{II/II}- β starting material. However, the edge of the X samples lies at a lower energy than for samples of the μ -oxo-Fe₂^{III/III} product. This phenomenon, also observed by Riggs-Gelasco et al.,^{11e} may result from the contribution of the unreacted Fe₂^{II/II} component in the freeze-quenched samples of X. Alternatively, the skewing of the edge energy to a lower value may be a feature inherent to X that remains to be explained theoretically.

Fe K-edge EXAFS data over photoelectron wave vector (k) = 0.3–14 \AA^{-1} (for samples containing the Fe₂^{II/II} reactant complex and the μ -oxo-Fe₂^{III/III} product state) and k = 0.3–16 \AA^{-1} (for samples containing X) are shown in Figure 1, along with fits to the raw data based on the parameters given in Tables 1 and S1–S3. The EXAFS data of the Fe₂^{II/II} reactant complex (Figure 1A, left panel) are best fit with a model that contains a total

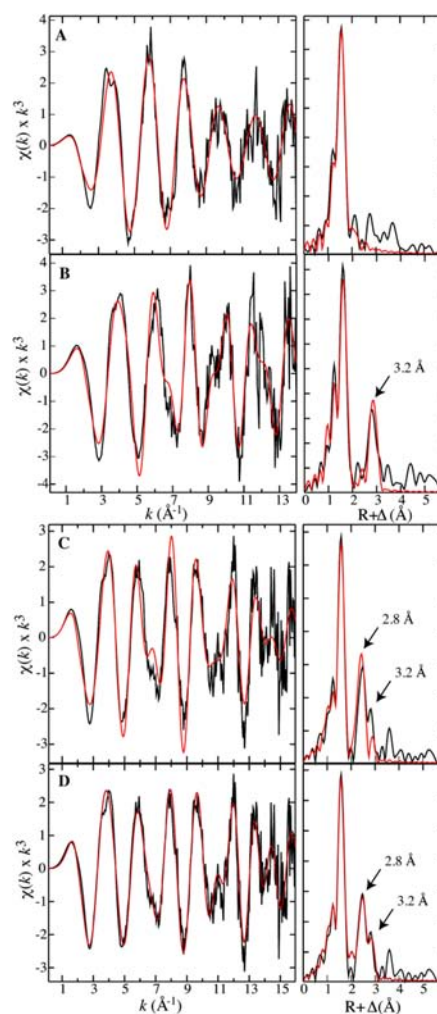


Figure 1. Fe K-edge EXAFS data (left) and their FTs (right) for samples containing the Fe₂^{II/II} reactant complex (A), the μ -oxo-Fe₂^{III/III} product (B) and X (C,D). Fit parameters are provided in Tables 1 and S1–S3.

Table 1. Fe K-Edge EXAFS ($k = 0.3–16 \text{ \AA}^{-1}$) Fitting Results for Samples Containing X^a

scatterer type	N	R (Å)	σ^2 (Å ²)
Fe–O/N	5	2.02	0.0097
Fe–O	0.65	1.75	0.0020
Fe–C	3	2.97	0.0046
Fe–C	1	3.24	0.0060
Fe–Fe	0.65	2.79	0.0033
Fe–Fe ^b	0.18	3.22	0.0043
F			0.366
E_0 (eV)			−11.067
resolution (Å)			0.099

^aOccupancies (N) were fixed during the fit, but distances (R), Debye–Waller factors (σ^2), and threshold energy shift (E_0) were allowed to vary. F is the fit error. ^bParameters for this scattering interaction were constrained to the values obtained from fits of the μ -oxo-Fe₂^{III/III} EXAFS data.

coordination number of four O/N ligands per Fe. This value is consistent with the crystal structure of that enzyme form.¹⁷ There is no evidence for an Fe–Fe scatterer in the Fourier transform (FT) of the EXAFS (Figure 1A, right panel), presumably because $d_{\text{Fe–Fe}}$ is too large ($\sim 3.8 \text{ \AA}$)¹⁷ in this form of the cluster. The EXAFS data for the μ -oxo-Fe₂^{III/III} product

cluster (Figure 1B, left panel) can be fit with a model that contains six O/N ligands per Fe.¹⁸ Furthermore, the FT of the EXAFS data exhibits a prominent Fe scattering interaction at $R = 3.2$ Å (Figure 1B, right panel), a value that is also consistent with the reported $d_{\text{Fe-Fe}}$ of this form.¹⁹

The EXAFS data for the samples containing X (Figure 1C, left panel) can be fit by a model with three O/N at 2.01 Å, two O/N at 2.11 Å, and 0.65 O at 1.75 Å per Fe. This fit also includes two Fe–Fe scattering interactions: 0.65 Fe at 2.78 Å, and 0.18 Fe at 3.22 Å (Table S3). The occupancies of the two Fe–Fe scattering interactions account for the heterogeneity of the sample, specifically the fractions of X and μ -oxo- $\text{Fe}_2^{\text{III/III}}$ cluster determined from the Mössbauer data. The contribution to the Fe–Fe scattering interactions in the EXAFS data from the $\sim 18\%$ $\text{Fe}_2^{\text{II/II}}$ component in the samples is not obvious and is not accounted for in the analysis. The Fe–O/N interaction at 1.75 Å is likely to arise from an oxo bridge, and the occupancy of 0.65 is consistent with the presence of two such μ -oxo interactions in an asymmetric di- μ -oxo- Fe_2 core (see Table S3 for additional fitting results).

The agreement between the fit and the data at $R \gtrsim 3.0$ Å can be improved by including additional non-nearest-neighbor scattering interactions. Examination of the crystal structures of the reactant and product complexes reveals the presence of C atoms from the bridging and terminal carboxylates and histidines that could contribute to scattering interactions at ~ 3.0 and ~ 3.2 Å. In the crystal structure of the $\text{Fe}_2^{\text{III/III}}$ product state (1RIB), there are a total of six Cs (three per Fe) at ~ 3.0 Å and two Cs (one per Fe) at 3.2 Å away from the Fe ions.¹⁸ Assuming that these atoms might also be present at similar distances in the samples containing X, we included three Fe–C scattering interactions at 3.0 Å and one at 3.2 Å into the fit model. Their inclusion significantly improves the agreement between the fit and the data (Figure 1D; parameters provided in Table 1). It is unclear why these interactions would be required for fits of the EXAFS data for X but not the μ -oxo- $\text{Fe}_2^{\text{III/III}}$ product. It is possible that the high-valent X contains a tighter core, making these scattering interactions pronounced. Irrespective of the origin of the additional interactions, the dominant scattering interaction at ~ 2.8 Å can be assigned to an Fe scatterer, and there is no evidence for an interaction at the previously reported $d_{\text{Fe-Fe}} \approx 2.5$ Å.

To determine the structure of the diiron core of X and rationalize the 2.8 Å $d_{\text{Fe-Fe}}$, we generated a series of structural models by broken-symmetry (BS) DFT methods, following previous work by Noodleman and coworkers.¹² (see Supporting Information for a more detailed description). The models were derived from the X-ray crystallographic data (1RIB) for *Ec* β by modifying the ligation. Two main candidates were examined in detail, a di- $(\mu$ -oxo)- $(\mu$ -1,3-carboxylato) core structure and a $(\mu$ -oxo) $(\mu$ -hydroxo) $(\mu$ -1,3-carboxylato) structure (Figure 2). The di- μ -oxo model has distance parameters that closely match the experimentally determined values, including, most notably, $d_{\text{Fe-Fe}} = 2.8$ Å (Figure 2).

Notably, the DFT calculations imply that protonating one of the μ -oxo bridges should result in an elongation of $d_{\text{Fe-Fe}}$ to ~ 3.0 Å, where a minor scatterer is detectable in the data. The results of magnetic circular dichroism studies on X suggested a model in which one of the bridging oxo groups is protonated.^{11b} Including an Fe scatterer at ~ 3.0 Å (in lieu of additional C scatterers at 3.0 and 3.2 Å) also improves the fit in this region. However, such a structure is inconsistent with data from ²H electron–nuclear

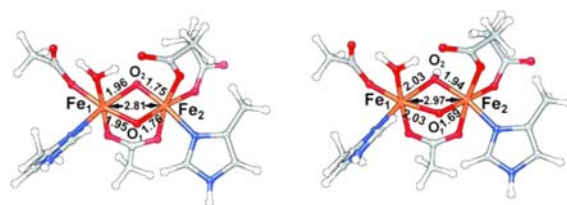


Figure 2. Structural models for the $\text{Fe}_2^{\text{III/IV}}$ core of X derived from BS DFT calculations. Left, $(\mu$ -oxo)₂ core; right, $(\mu$ -oxo) $(\mu$ -hydroxo) core.

double resonance experiments, which do not detect a hydron from a μ -hydroxo ligand.^{11d,fg}

The effect of including the essential Y_{122} that is oxidized by X in the DFT calculations was also evaluated (see Supporting Information for details of the computational methodology). Y_{122} forms a H bond to aspartate 84, which ligates Fe1 of the Fe–Fe cluster. Its presence provides a potential proton-transfer pathway by which one of the μ -oxo bridges in X might be protonated, thereby altering the core structure of the intermediate. The results of our DFT calculations, like those of Noodleman and coworkers, show that the presence of Y_{122} has a minor effect on the optimized geometries, resulting in only a slight increase (~ 0.02 Å) in $d_{\text{Fe-Fe}}$ (Table S9). It seems unlikely that the structure of X in the β - Y_{122} F variant could be significantly different from that formed in the wild-type protein.

In an effort to understand the basis for the discrepancy between the $d_{\text{Fe-Fe}}$ values of 2.8 Å determined here and the previously reported 2.5 Å, we considered that third-generation synchrotron technology and the increased (2.5 \times) concentration of X (obtained through the use of Cl₂ and ClO₂[−]) could result in a critical increase in signal-to-noise ratio. Interestingly, this was not the case. The data from the two studies have effectively the same signal-to-noise ratio. We also considered that the increased resolution provided by the extended k -range of our measurements might be critical to the observation of $d_{\text{Fe-Fe}} = 2.8$ Å. Whereas the data analyzed in the previous study were limited to $k = 2$ –12.6 Å^{−1}, the data reported here were fit from $k = 0.3$ –16 Å^{−1}. To evaluate whether this difference might be a plausible explanation for the discrepant results, we examined FTs of unfiltered EXAFS data with cutoffs at $k = 11, 12, 13, 14, 15,$ and 16 Å^{−1}. Figure 3 shows that the intensity of the 2.8 Å peak does decrease with k , becoming a shoulder when $k_{\text{max}} = 11.0$ Å^{−1}. However, fits over five of the six k ranges listed in Figure 3 yield $d_{\text{Fe-Fe}} = 2.8$ Å (fits of the shortest range, $k = 0$ –11 Å^{−1}, yield $d_{\text{Fe-Fe}} = 2.37$ Å, with a large Debye–Waller factor of 0.01 Å²). In no case does truncating our data lead to the assignment of a 2.5 Å Fe–Fe scattering interaction. It appears that the data reported here and in the previous study are inherently different, suggesting that they were obtained from inherently different samples (i.e., not from the same species). To illustrate this point, we overlay the EXAFS data obtained from both studies in Figure S8.

This re-examination of the structure of X and subsequent upward adjustment of its $d_{\text{Fe-Fe}}$ calls into question the short $d_{\text{Fe-Fe}}$ values reported for other O₂-derived diiron reaction intermediates. For example, the high-valent $\text{Fe}_2^{\text{IV/IV}}$ complex, Q, that accumulates during the conversion of methane to methanol by the soluble methane monooxygenase from *Methylosinus trichosporium* OB3b was characterized by EXAFS spectroscopy, and the measured $d_{\text{Fe-Fe}} = 2.46$ Å led to the proposal of a $[(\mu$ -oxo)₂Fe₂] “diamond core” structure.²⁰ Subsequently, EXAFS characterization of the μ -peroxo- $\text{Fe}_2^{\text{III/III}}$ complexes that accumulate in the reactions of M ferritin from frog²¹ and the

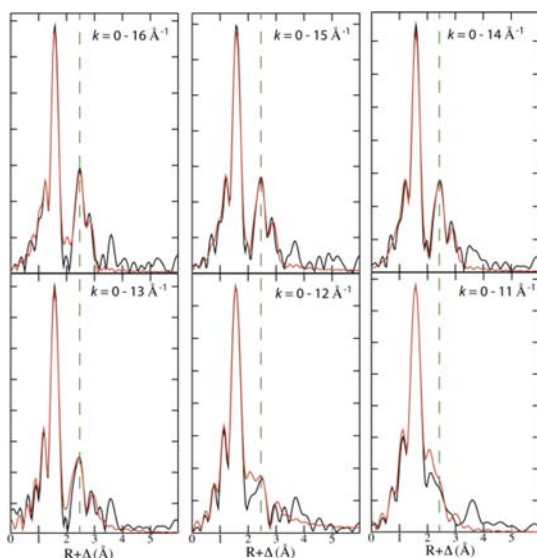


Figure 3. FT of EXAFS data for samples containing X plotted with different cutoffs of the k -range. The dashed line is drawn at the middle of the ~ 2.8 Å peak. Overlaid in red is the FT resulting from the fit reported in Table 1.

$D_{84}E/W_{48}A$ variant of *Ec* RNR- β^{22} led to reports of similar values of d_{Fe-Fe} (~ 2.5 Å) even in these mid-valent complexes. In general, the structures dictated by these surprisingly short d_{Fe-Fe} values have been irreconcilable with synthetic and computational models, which predict $d_{Fe-Fe} \approx 2.7$ Å for Q and >3.0 Å for the μ -peroxo- $Fe_2^{III/III}$ complexes.²³ Re-examination of these other complexes and re-determination of their d_{Fe-Fe} values would seem to be warranted.

■ ASSOCIATED CONTENT

Supporting Information

Sample preparation, Mössbauer and EXAFS spectra, fits to the data, computational methodology, and tables. This material is available free of charge via the Internet at <http://pubs.acs.org>.

■ AUTHOR INFORMATION

Corresponding Author

ckrebs@psu.edu; jmb21@psu.edu; mtg10@psu.edu

Present Addresses

[§]Department of Molecular Biosciences, Northwestern University, Evanston, IL

[#]Department of Chemistry, Stanford University, Stanford, CA

Notes

The authors declare no competing financial interest.

■ ACKNOWLEDGMENTS

This work was supported by the National Institutes of Health (GM-55365 to J.M.B., C.K., and M.T.G.) and an Alfred P. Sloan Minority Ph.D. fellowship to L.M.K.D.

■ REFERENCES

- (1) (a) Nordlund, P.; Reichard, P. *Annu. Rev. Biochem.* **2006**, *75*, 681. (b) Stubbe, J. *Curr. Opin. Struct. Biol.* **2000**, *10*, 731.
- (2) Licht, S.; Gerfen, G. J.; Stubbe, J. *Science* **1996**, *271*, 477.
- (3) (a) Stubbe, J.; Nocera, D. G.; Yee, C. S.; Chang, M. C. Y. *Chem. Rev.* **2003**, *103*, 2167. (b) Stubbe, J.; Riggs-Gelasco, P. *Trends Biochem. Sci.* **1998**, *23*, 438.

(4) Atkin, C. L.; Thelander, L.; Reichard, P.; Lang, G. J. *Biol. Chem.* **1973**, *248*, 7464.

(5) (a) Tong, W. H.; Chen, S.; Lloyd, S. G.; Edmondson, D. E.; Huynh, B. H.; Stubbe, J. *J. Am. Chem. Soc.* **1996**, *118*, 2107. (b) Yun, D.; Garcia-Serres, R.; Chicalese, B. M.; An, Y. H.; Huynh, B. H.; Bollinger, J. M., Jr. *Biochemistry* **2007**, *46*, 1925. (c) Bollinger, J. M., Jr.; Krebs, C.; Vicol, A.; Chen, S.; Ley, B. A.; Edmondson, D. E.; Huynh, B. H. *J. Am. Chem. Soc.* **1998**, *120*, 1094.

(6) Baldwin, J.; Krebs, C.; Ley, B. A.; Edmondson, D. E.; Huynh, B. H.; Bollinger, J. M., Jr. *J. Am. Chem. Soc.* **2000**, *122*, 12195.

(7) Bollinger, J. M., Jr.; Edmondson, D. E.; Huynh, B. H.; Filley, J.; Norton, J. R.; Stubbe, J. *Science* **1991**, *253*, 292.

(8) Wu, C. H.; Jiang, W.; Krebs, C.; Stubbe, J. *Biochemistry* **2007**, *46*, 11577.

(9) Ravi, N.; Bollinger, J. M., Jr.; Huynh, B. H.; Edmondson, D. E.; Stubbe, J. *J. Am. Chem. Soc.* **1994**, *116*, 8007.

(10) Stubbe, J. *Curr. Opin. Chem. Biol.* **2003**, *7*, 183.

(11) (a) Mitić, N.; Saleh, L.; Schenk, G.; Bollinger, J. M., Jr.; Solomon, E. I. *J. Am. Chem. Soc.* **2003**, *125*, 11200. (b) Mitić, N.; Clay, M. D.; Saleh, L.; Bollinger, J. M., Jr.; Solomon, E. I. *J. Am. Chem. Soc.* **2007**, *129*, 9049. (c) Sturgeon, B. E.; Burdi, D.; Chen, S.; Huynh, B. H.; Edmondson, D. E.; Stubbe, J.; Hoffman, B. M. *J. Am. Chem. Soc.* **1996**, *118*, 7551. (d) Shanmugam, M.; Doan, P. E.; Lees, N. S.; Stubbe, J.; Hoffman, B. M. *J. Am. Chem. Soc.* **2009**, *131*, 3370. (e) Riggs-Gelasco, P. J.; Shu, L.; Chen, S.; Burdi, D.; Huynh, B. H.; Que, L., Jr.; Stubbe, J. *J. Am. Chem. Soc.* **1998**, *120*, 849. (f) Burdi, D.; Sturgeon, B. E.; Tong, W. H.; Stubbe, J.; Hoffman, B. M. *J. Am. Chem. Soc.* **1996**, *118*, 281. (g) Burdi, D.; Willems, J.-P.; Riggs-Gelasco, P.; Antholine, W. E.; Stubbe, J.; Hoffman, B. M. *J. Am. Chem. Soc.* **1998**, *120*, 12910.

(12) (a) Han, W.-G.; Liu, T.; Lovell, T.; Noodleman, L. *J. Am. Chem. Soc.* **2005**, *127*, 15778. (b) Han, W.-G.; Liu, T.; Lovell, T.; Noodleman, L. *J. Inorg. Biochem.* **2006**, *100*, 771. (c) Han, W.-G.; Liu, T.; Lovell, T.; Noodleman, L. *Inorg. Chem.* **2006**, *45*, 8533. (d) Han, W.-G.; Noodleman, L. *Dalton Trans.* **2009**, 6045. (e) Han, W.-G.; Noodleman, L. *Theor. Chem. Acc.* **2010**, *125*, 305.

(13) Neese, F. *J. Biol. Inorg. Chem.* **2006**, *11*, 702.

(14) (a) Zang, Y.; Dong, Y.; Que, L., Jr.; Kauffmann, K.; Münck, E. *J. Am. Chem. Soc.* **1995**, *117*, 1169. (b) Dong, Y.; Fujii, H.; Hendrich, M. P.; Leising, R. A.; Pan, G.; Randall, C. R.; Wilkinson, E. C.; Zang, Y.; Que, L., Jr.; Fox, B. G.; Kauffman, K.; Münck, E. *J. Am. Chem. Soc.* **1995**, *117*, 2778. (c) Hsu, H.-F.; Dong, Y.; Shu, L.; Young, V. G.; Que, L., Jr. *J. Am. Chem. Soc.* **1999**, *121*, 5230.

(15) Younker, J. M.; Krest, C. M.; Jiang, W.; Krebs, C.; Bollinger, J. M., Jr.; Green, M. T. *J. Am. Chem. Soc.* **2008**, *130*, 15022.

(16) Dassama, L. M. K.; Yosca, T. H.; Conner, D. A.; Lee, M. H.; Blanc, B.; Streit, B. R.; Green, M. T.; DuBois, J. L.; Krebs, C.; Bollinger, J. M., Jr. *Biochemistry* **2012**, *51*, 1607.

(17) Logan, D. T.; Su, X.-D.; Åberg, A.; Regnström, K.; Hajdu, J.; Eklund, H.; Nordlund, P. *Structure* **1996**, *4*, 1053.

(18) Nordlund, P.; Eklund, H. *J. Mol. Biol.* **1993**, *232*, 123.

(19) (a) Scarrow, R. C.; Maroney, M. J.; Palmer, S. M.; Que, L., Jr.; Salowe, S. P.; Stubbe, J. *J. Am. Chem. Soc.* **1986**, *108*, 6832. (b) Scarrow, R. C.; Maroney, M. J.; Palmer, S. M.; Que, L., Jr.; Roe, A. L.; Salowe, S. P.; Stubbe, J. *J. Am. Chem. Soc.* **1987**, *109*, 7857.

(20) Shu, L.; Nesheim, J. C.; Kauffmann, K. E.; Münck, E.; Lipscomb, J. D.; Que, L., Jr. *Science* **1997**, *275*, 515.

(21) Hwang, J.; Krebs, C.; Huynh, B. H.; Edmondson, D. E.; Theil, E. C.; Penner-Hahn, J. E. *Science* **2000**, *287*, 122.

(22) Baldwin, J.; Krebs, C.; Saleh, L.; Stelling, M.; Huynh, B. H.; Bollinger, J. M., Jr.; Riggs-Gelasco, P. *Biochemistry* **2003**, *42*, 13269.

(23) (a) Gherman, B. F.; Baik, M.-H.; Lippard, S. J.; Friesner, R. A. *J. Am. Chem. Soc.* **2004**, *126*, 2978. (b) Xue, G.; Wang, D.; De Hont, R.; Fiedler, A. T.; Shan, X.; Münck, E.; Que, L., Jr. *Proc. Natl. Acad. Sci. U.S.A.* **2007**, *104*, 20713. (c) Cranswick, M. A.; Meier, K. K.; Shan, X.; Stubna, A.; Kaizer, J.; Mehn, M. P.; Münck, E.; Que, L., Jr. *Inorg. Chem.* **2012**, *51*, 10417. (d) Han, W.-G.; Noodleman, L. *Inorg. Chim. Acta* **2008**, *361*, 973.